ISSN 1063-7788, Physics of Atomic Nuclei, 2020, Vol. 83, No. 1, pp. 1–8. © Pleiades Publishing, Ltd., 2020.
Russian Text © The Author(s), 2020, published in Yadernaya Fizika, 2020, Vol. 83, No. 1, pp. 2–9.

NUCLEI
Experiment

Photoneutron Reactions on ^{129}Xe Nuclei and Their Electromagnetic Dissociation in Colliders

S. S. Belyshev[1)], V. V. Varlamov[2)], S. A. Gunin[3),4)], A. I. Davydov[1)], B. S. Ishkhanov[1),2)], I. A. Pshenichnov[4)*], and V. N. Orlin[2)]

Received May 3, 2019; revised June 16, 2019; accepted June 16, 2019

Abstract—The electromagnetic dissociation of ultrarelativistic nuclei has a substantial impact on the lifetime of beams in the Relativistic Heavy Ion Collider (RHIC) and Large Hadron Collider (LHC), and secondary nuclei produced upon this dissociation may have an adverse effect on collider components. At the same time, the detection of neutrons originating from the electromagnetic dissociation process makes it possible to monitor the luminosity of colliders. In order to calculate the total and partial cross sections for the electromagnetic dissociation process by the Weizsäcker–Williams method, one needs reliable photonuclear reaction models preliminarily tested via a comparison of the results that they produce with available experimental data. Since the commissioning of the LHC, attention has been given primarily to ^{208}Pb–^{208}Pb collisions. A run involving ^{129}Xe nuclei was also performed. In contrast to the case of ^{208}Pb nuclei, for which the photonuclear reaction and electromagnetic dissociation cross sections have been measured at various laboratories, there are no data for ^{129}Xe. By employing the experimental–theoretical method, the $(\gamma, 1n)$, $(\gamma, 2n)$, $(\gamma, 3n)$, and (γ, abs) cross sections for the ^{129}Xe nucleus are evaluated on the basis of available data for the neighboring nucleus of ^{127}I and the combined photonuclear reaction model (CPNRM). It is found that the results of CPNRM calculations performed for ^{129}Xe at photon energies up to 40 MeV by employing the TENDL-2017 library compiled by means of the TALYS code are close to one another and are in fairly good agreement with data obtained at the Saclay laboratory for ^{127}I. These new evaluated data, the TENDL-2017 library, and approximations of the total photoabsorption cross sections above the pion production threshold are used to calculate the electromagnetic dissociation cross section for ^{129}Xe at the LHC and at the FCC-hh collider being designed. The results of these calculations are compared with their counterparts obtained on the basis of the RELDIS model.

DOI: 10.1134/S1063778819060036

1. INTRODUCTION

Hot and dense nuclear matter is formed in the region of overlap of spatial distributions of nuclear densities of colliding ultrarelativistic nuclei. Since the highest energy density is generated by the interaction of a significant number of intranuclear nucleons from either nuclear partner in the collision process, a key role in the research programs for the Relativistic Heavy Ion Collider (RHIC) at the Brookhaven National Laboratory (USA) and the Large Hadron collider (LHC) at CERN is played by investigations into collisions of heavy nuclei—^{197}Au–^{197}Au collisions at RHIC [1] and ^{208}Pb–^{208}Pb collisions at the LHC [2]. The interactions of oxygen, sulfur, argon, xenon, indium, and lead nuclei accelerated at the Super Proton Synchrotron (SPS) with light and heavy target nuclei have been studied in various years at CERN [3]. In particular, the properties of nucleus–nucleus collisions at various energies versus the masses of colliding nuclei are being systematically studied in the NA61/SHINE experiment [4]. The injection of nuclei into the LHC that have different masses and charges requires, in addition to thoroughly retuning the collider itself [5], the readjustment of the whole preaccelerator system and the ion storage ring: LINAC3, LEIR, PS, and SPS. This is one of the reasons why, since the commissioning of the LHC in 2010, ^{129}Xe nuclei were accelerated only once in addition to the acceleration of protons and ^{208}Pb nuclei. In the future, after the completion of collider upgrade in 2021 (HL-LHC project)—or later, after the replacement of magnets with the aim of

[1)]Faculty of Physics, Lomonosov Moscow State University, Moscow, 119991 Russia.
[2)]Skobeltsyn Institute of Nuclear Physics, Lomonosov Moscow State University, Moscow, 119991 Russia.
[3)]Moscow Institute of Physics and Technology (State University), Moscow oblast, 141700 Russia.
[4)]Institute for Nuclear Research, Russian Academy of Sciences, Moscow, 117312 Russia.
[*]E-mail: pshenich@inr.ru

increasing the collision energy (HE-LHC project)—the set of nuclei accelerated at the LHC will probably be broadened via adding lighter nuclei, such as ^{16}O, ^{40}Ar, ^{40}Ca, and ^{78}Kr [6]. In the ion source used at CERN [7], which is based on the electron cyclotron resonance, it is convenient to apply inert gases; therefore, ^{40}Ar, ^{78}Kr, ^{84}Kr, and ^{129}Xe are the main candidates for use in future experiments.

In addition to the need for studying the physics of nucleus–nucleus collisions versus the size of colliding nuclei, the use of nuclei lighter than ^{208}Pb would permit reducing the loss of beam nuclei via electromagnetic processes. Indeed, the electromagnetic dissociation (EMD) of ^{208}Pb under the impact of the Lorentz-contracted Coulomb fields of nuclear partners in ultraperipheral collisions, along with the pickup of electrons by ^{208}Pb from e^+e^- pairs produced in these intense fields, causes a significant loss of nuclei from collider beams [8]. In contrast to what occurs in the fragmentation of nuclei in hadron interaction, secondary ions characterized by charge-to-mass ratios close to that for ^{208}Pb are frequently formed in electromagnetic processes. Such ions may pass through the system of LHC collimators and have adverse radiation and thermal effects on the LHC components [8]. Reliable values of the partial cross sections for the emission of one and two neutrons in EMD of ^{208}Pb are necessary for monitoring the LHC luminosity by detecting these neutrons in the forward Zero Degree Calorimeters (ZDC) [9]. As was shown in [10], the RELDIS model [9], which relies on the Weizsäcker–Williams method [11] and which simulates nucleon emission from ^{208}Pb nuclei on the basis of the Monte Carlo method, describes well data from the ALICE experiment at the LHC on neutron emission in the EMD process.

In order to calculate total and partial cross sections for EMD processes by the Weizsäcker–Williams method, it is necessary to have reliable photonuclear reaction models preliminarily tested by comparing the results obtained on their basis with experimental data. However, there are no relevant data on ^{129}Xe nuclei; on the whole, the ^{129}Xe nucleus has not yet received adequate study. Therefore, it was proposed, for example, in [12] to use the differential cross sections measured for ρ^0-meson photoproduction in ultraperipheral collisions of ^{129}Xe nuclei at the LHC in order to determine the nuclear density distribution in these nuclei and their radii.

The objective of the present study is to evaluate the $(\gamma, 1n)$, $(\gamma, 2n)$, $(\gamma, 3n)$, and $(\gamma,$ abs) cross sections for the ^{129}Xe nucleus by means of the experimental–theoretical method on the basis of data available for the neighboring nucleus of ^{127}I and the combined photonuclear reaction model (CPNRM) [13, 14]. With the aid of the new evaluated data that are obtained in this way, the TENDL-2017 library developed on the basis of the TALYS code [15], and approximations of total photoabsorption cross sections in the region above the pion production threshold [16], we then calculate the EMD cross sections for collisions of ^{129}Xe nuclei at the LHC and at the FCC-hh collider being designed [17] and compare these results with their counterparts obtained on the basis of the RELDIS model [9].

2. COMPARISON OF THEORETICAL PHOTONEUTRON REACTION CROSS SECTIONS FOR THE ^{129}Xe NUCLEUS WITH EXPERIMENTAL DATA FOR NEIGHBORING NUCLEI

Since there are no experimental data on photoneutron reaction cross sections for the ^{129}Xe nucleus, calculations within the CPNRM framework [13, 14] are performed in the present study for ^{129}Xe by employing data from the TENDL-2017 library that were obtained with the aid of the TALYS code [15]. The partial cross sections are calculated for reactions involving the emission of various numbers of neutrons—$(\gamma, 1nX)$, $(\gamma, 2nX)$, and $(\gamma, 3nX)$, where X indicates the possible presence of charged final state particles in addition to neutrons (for the sake of brevity, X is omitted in the following)—along with their sum, which is the total photoneutron cross section

$$\sigma(\gamma, Sn) = \sigma(\gamma, 1n) + \sigma(\gamma, 2n) + \sigma(\gamma, 3n) + \ldots. \quad (1)$$

For heavy nuclei, this sum provides a good approximation of the total photoabsorption cross section, $\sigma(\gamma, \text{abs}) \approx \sigma(\gamma, Sn)$. These cross sections and the inclusive neutron yield cross section

$$\sigma(\gamma, xn) = \sigma(\gamma, 1n) + 2\sigma(\gamma, 2n) + 3\sigma(\gamma, 3n) + \ldots \quad (2)$$

are compared with data on the photodisintegration of nuclei neighboring ^{129}Xe, such as ^{127}I [18, 19], ^{128}Te [20], ^{133}Cs [21, 22], and ^{138}Ba [23]. These data were obtained with beams of quasimonoenergetic annihilation photons by means of the photoneutron multiplicity sorting method.

It was found that, for all of the partial and total reactions being considered, the results of the calculations performed for the ^{129}Xe nucleus within the CPNRM framework and by means of the TALYS code are close to each other and that agreement of the reaction cross sections calculated for the ^{129}Xe nucleus with their experimental counterparts turns out to be the best for the data obtained for the ^{127}I

nucleus at the Saclay nuclear center (France) [19]. A comparison of the reaction cross sections in question for the ^{127}I and ^{129}Xe nuclei is illustrated in Fig. 1. This figure shows that there are substantial systematic discrepancies between the experimental results from [18] and [19].

The results of the aforementioned comparison permit employing the inclusive neutron yield cross section in (2) for the ^{127}I nucleus from [19] and the results of theoretical calculations for the ^{129}Xe nucleus within the CPNRM framework [13, 14] to evaluate the partial cross sections and the total photoneutron cross section for the ^{129}Xe nucleus.

3. EVALUATION OF THE PHOTONEUTRON REACTION CROSS SECTIONS FOR THE ^{129}Xe NUCLEUS BY MEANS OF THE EXPERIMENTAL–THEORETICAL METHOD

In order to determine the cross sections for partial photoneutron reactions on the ^{129}Xe nucleus from the experimental data on the neutron yield cross section for the neighboring nucleus of ^{127}I, we employ the experimental–theoretical method for evaluating partial reaction cross sections that would be independent of the systematic uncertainties of the experimental method of photoneutron multiplicity sorting. Earlier, this method was successfully applied to photoneutron reactions on various nuclei [24–34]. Within this method, the cross sections for reactions in which final state neutrons have various multiplicity values ($i = 1$, 2, 3, ...) are evaluated according to the relations

$$\sigma^{\text{eval}}(\gamma, in) = F_i^{\text{theor}}\sigma^{\text{exp}}(\gamma, xn) \qquad (3)$$

by employing the theoretical transition neutron multiplicity functions

$$F_i^{\text{theor}} = \sigma^{\text{theor}}(\gamma, in)/\sigma^{\text{theor}}(\gamma, xn), \qquad (4)$$

calculated within the CPNRM framework [13, 14]. Relation (3) means that the experimental inclusive neutron yield cross section in (2), which is independent of the experimental uncertainties in neutron multiplicity sorting owing to taking into account all of the emitted neutrons, is split into the contributions of the partial reactions according to equations of this model that determine the transition neutron multiplicity functions F_i^{theor} in (4). These functions are also independent of the problems of experimental photoneutron multiplicity sorting. On the basis of the results obtained earlier for more than 30 nuclei, it was shown that the cross sections evaluated for partial photoneutron reactions by means of the above method turn out to be free from the systematic uncertainties of experimental methods and are therefore reliable [24–34].

The $(\gamma, 1n)$, $(\gamma, 2n)$, and $(\gamma, 3n)$ cross sections and the total photoneutron reaction cross section $\sigma(\gamma, Sn)$ (1) for the ^{129}Xe nucleus were evaluated by means of the experimental–theoretical method outlined above. In doing this, we used experimental data on the inclusive photoneutron yield cross section for the ^{127}I nucleus [19]. The numerical values were obtained on the basis of the international digital database of nuclear reaction cross sections in [35]. In this database, the $(\gamma, 1n)$ cross section is presented up to the energy of 22.5 MeV, while the neutron yield cross section $\sigma(\gamma, xn)$ (2) is given up to 25 MeV; at the same time, the $(\gamma, 2n)$ and $(\gamma, 3n)$ cross sections are given up to the energy of 31.2 MeV. Within the procedure for evaluating expression (3), the respective sum (2) of the experimental cross sections for the $(\gamma, 1n)$, $(\gamma, 2n)$, and $(\gamma, 3n)$ partial reactions was therefore used [18]. This made it possible to perform an evaluation in the energy region extending up to 31.2 MeV. The ratios F_i^{theor} used in the procedure for evaluating expression (3) were calculated within the CPNRM framework [24, 25].

The cross sections evaluated for partial reactions and for the total photoneutron reaction (1) are given in Fig. 2. Also shown in this figure for the sake of comparison are the Livermore data from [18] and the results obtained on the basis of the RELDIS model [9]. It is noteworthy that this model employs the systematics of total photoabsorption cross sections from [36], which, for the ^{127}I nucleus, is nearly coincident with the Livermore data from [18], which, in turn, fall short of the Saclay data from [19]. Figure 2 also shows that the RELDIS model underestimates the $(\gamma, 2n)$ cross section in the vicinity of the threshold. The respective integrated cross sections for the reactions being discussed are compiled in Table 1, from which it can be seen that the evaluated data on the integrated cross sections are rather close to the Saclay data from [19].

4. TOTAL EMD CROSS SECTIONS FOR ^{129}Xe AT THE LHC AND FCC-hh

The data on the total cross section for the photodisintegration of the ^{129}Xe nucleus in the photon-energy range from the neutron emission threshold to 31 MeV that were evaluated for the first time in the present study make it possible to calculate the total EMD cross section for ^{129}Xe nuclei at the LHC and FCC-hh upon supplementing these data with the cross sections in the region above 31 MeV from the TENDL-2017 library, which were obtained with the aid of the TALYS code [15] to the pion photoproduction threshold at 140 MeV, and with the approximations of the total photoabsorption cross sections for nuclei [16] above this threshold. Indeed,

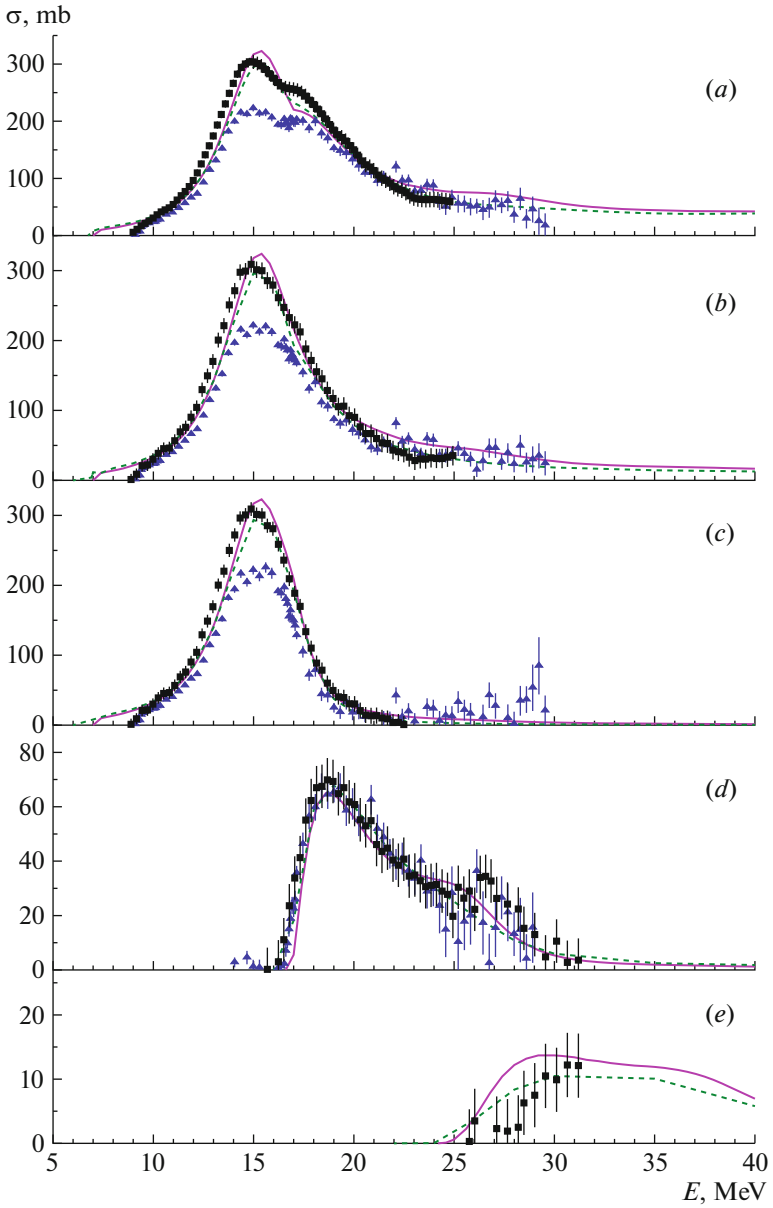

Fig. 1. Theoretical reaction cross sections for the ^{129}Xe nucleus (solid curve) from [13, 14] and (dashed curve) from [15] along with the respective experimental cross sections for the ^{127}I nucleus (closed triangles) from [18] and (closed boxes) from [19]: (*a*) $\sigma(\gamma, xn)$, (*b*) $\sigma(\gamma, Sn)$, (*c*) $\sigma(\gamma, 1n)$, (*d*) $\sigma(\gamma, 2n)$, and (*e*) $\sigma(\gamma, 3n)$.

measurements reported in [10] confirmed that, owing to the dominance of soft equivalent photons in the Weizsäcker–Williams photon-energy spectrum, the emission of one neutron saturates more than 50% of the EMD cross section for ^{208}Pb at the LHC; the two-neutron channel additionally contributes about 10%. This suggests that it would be natural to expect the dominance of the contribution of the one- and two-neutron channels to the total EMD cross section for ^{129}Xe as well.

Figure 3 illustrates the behavior of the total photoabsorption cross sections for the ^{129}Xe nucleus that are used in the present study to calculate the total cross sections for single EMD. Also given here is the convolution of these cross sections with the spectrum of equivalent photons. The total EMD cross section for ^{129}Xe nuclei in their collisions at colliders is obtained by integrating the convolution in question with respect to energy.

Depending on the photon energy, use was made of five approximations (versions I–V) of the total photoabsorption cross sections. In versions III and V, we took cross sections estimated in the present study for energies in the range of $E_\gamma < 31.2$ MeV, the data from the TENDL-2017 library in the range of

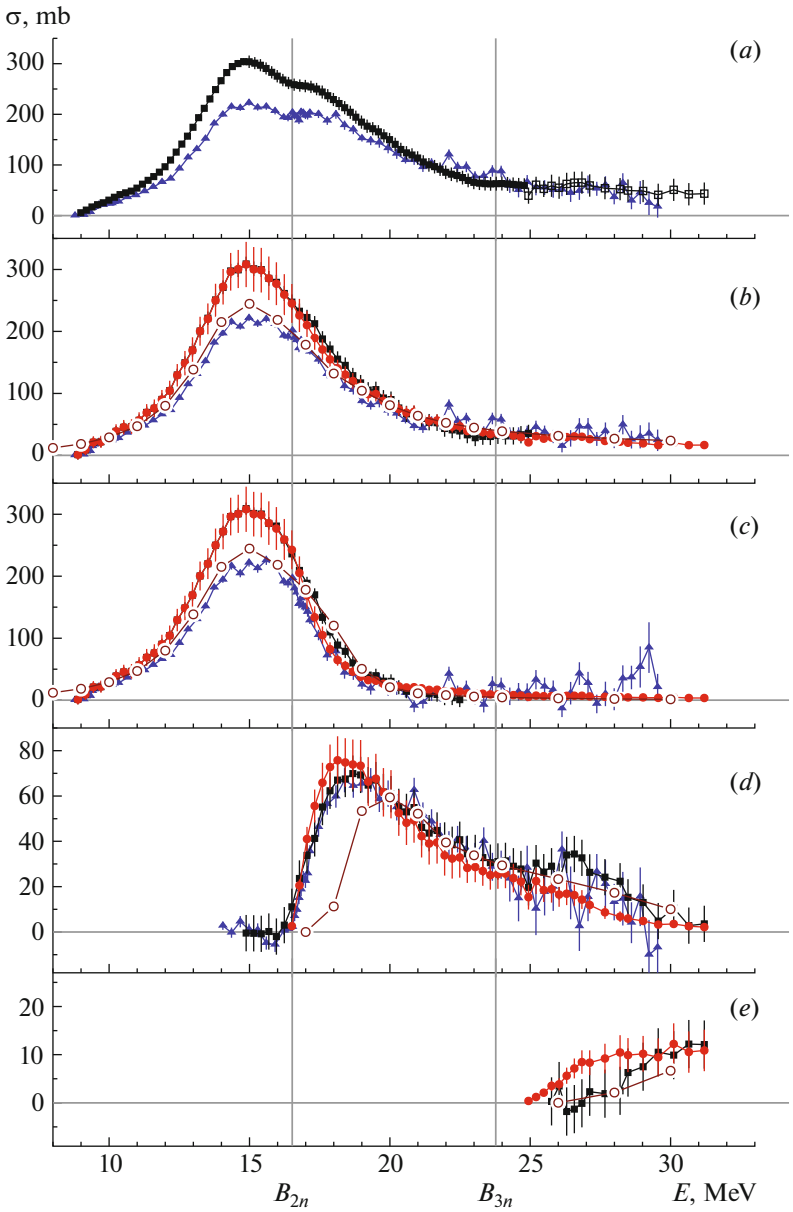

Fig. 2. Evaluated (circles) reaction cross sections for the ^{129}Xe nucleus along with experimental ([19], squares) reaction cross sections for the ^{127}I nucleus: (*a*) $\sigma(\gamma, xn)$, (*b*) $\sigma(\gamma, Sn)$, (*c*) $\sigma(\gamma, 1n)$, (*d*) $\sigma(\gamma, 2n)$, and (*e*) $\sigma(\gamma, 3n)$. The experimental data for $\sigma(\gamma, xn)$ were obtained from the database in [35] for energies of up to 25 MeV and as the sum (2) of the experimental data for the $(\gamma, 1n)$, $(\gamma, 2n)$, and $(\gamma, 3n)$ reactions from [35] at higher energies. Also shown in this figure are Livermore data (triangles) from [18] and the results obtained on the basis of the RELDIS model [9] (open circles).

31.2 MeV $< E_\gamma <$ 140 MeV, and the approximations from [16] for $E_\gamma >$ 145 MeV. In order to match the different approximations with one another, we employed linear interpolations between the extreme points of respective intervals. The data from the TENDL-2017 library are taken for the photoabsorption cross sections below 140 MeV in version I. In order to estimate the effect of growth of the total cross sections for nuclei in the region above 60 GeV (versions IV and V) on the EMD cross sections, we used different dependences (I, II, and III) in which the photoabsorption cross sections did not change above 60 GeV—Fig. 3 gives an example of such a dependence. In particular, the RELDIS model [9] disregards the growth of the cross section in the region of high energies (version I).

Tables 2 and 3 contain basic results of the present study—that is, the total cross sections calculated for single EMD of ^{129}Xe nuclei at the LHC and FCC-hh energies in the approximation of one-photon exchange on the basis of five approximations of the total photoabsorption cross section. It is noteworthy that

Table 1. Evaluated integrated neutron yield cross sections, total cross sections, and partial photoneutron cross sections (in MeV mb units) for the ^{129}Xe nucleus along with experimental data for the ^{127}I nucleus from [19, 35] at various values of the upper integration limit E^{int}, but for the same lower limit, which corresponds to the neutron emission threshold

Reaction	[19, 35]	Evaluation	[19, 35]	Evaluation	[19, 35]	Evaluation
	$E^{\text{int}} = B2n = 16.52$ MeV		$E^{\text{int}} = B3n = 23.85$ MeV		$E^{\text{int}} = 31.20$ MeV	
(γ, xn)*	1213.8 ± 10.9	1210.9 ± 24.0	2319.8 ± 18.7	2283.8 ± 31.6	2708.1 ± 25.3	2647.7 ± 33.5
(γ, Sn)	1210.6 ± 24.0	1212.5 ± 10.1	1960.8 ± 16.5	1929.1 ± 27.5	2139.5 ± 20.0	2105.7 ± 28.2
$(\gamma, 1n)$**	1210.6 ± 24.0	1211.1 ± 9.4	1601.7 ± 13.7	1574.4 ± 26.0	1601.7 ± 13.7	1615.5 ± 26.1
$(\gamma, 2n)$	0.3 ± 0.1	1.4 ± 3.8	359.1 ± 8.8	354.7 ± 9.0	506.9 ± 13.2	438.7 ± 9.9
$(\gamma, 3n)$	–	–	–	–	30.8 ± 5.6	51.6 ± 4.0

* The experimental data for this reaction were obtained from the database in [35] for energies of up to 25 MeV and as the sum (2) of the experimental data for the $(\gamma, 1n)$, $(\gamma, 2n)$, and $(\gamma, 3n)$ reactions in [35] at higher energies.
** The experimental data on the $(\gamma, 1n)$ cross section are available up to an energy of 22.5 MeV [19].

Table 2. Total cross sections for single electromagnetic dissociation in collisions of ^{129}Xe nuclei at the LHC according to calculations performed for various versions of total photoabsorption cross sections

^{129}Xe–^{129}Xe $\sqrt{s_{NN}} = 5.44$ TeV	RELDIS	TENDL-2017	Present study	TENDL-2017	Present study
	I	II	III	IV	V
EMD cross section (in barns)	50.3	54.0	53.8	54.8	54.6
Maximum photon energy (in TeV units)	251.6	251.9			
cross section growth for $E_\gamma > 60$ GeV	Absent	Absent	Absent	Present	Present

Table 3. Total cross sections for single electromagnetic dissociation in collisions of ^{129}Xe nuclei at the FCC-hh according to calculations performed for various versions of total photoabsorption cross sections

^{129}Xe–^{129}Xe $\sqrt{s_{NN}} = 41.8$ TeV	RELDIS	TENDL-2017	Present study	TENDL-2017	Present study
	I	II	III	IV	V
EMD cross section (in barns)	67.5	73.6	73.3	77.3	76.9
Maximum photon energy (in TeV units)	14845	14870			
cross section growth for $E_\gamma > 60$ GeV	Absent	Absent	Absent	Present	Present

the RELDIS model makes it possible to calculate additionally the two-photon exchange contribution, which, for the cases being considered, is 0.3 to 0.4 b (about 0.6%), but, for the comparison with the other versions of our calculations to be convenient, we did not include this contribution in the data in Tables 2 and 3. The upper boundaries of the equivalent-photon spectrum ($\sim\gamma/2R$) adopted in the present study and used in the RELDIS model are nearly identical, a moderately small difference stemming from the choice of radius R for the ^{129}Xe nucleus. As follows from these tables, the calculations on the basis of the TENDL-2017 library (II) lead to EMD cross sections that are 7 to 8% larger than their counterparts obtained on the basis of the RELDIS model (I), which employs the systematics from [36]. The use of our evaluated data (III) instead of TENDL-2017 data reduces insignificantly (by 0.4%) the calculated cross section. The effect associated with taking into account the growth of the cross section at high ener-

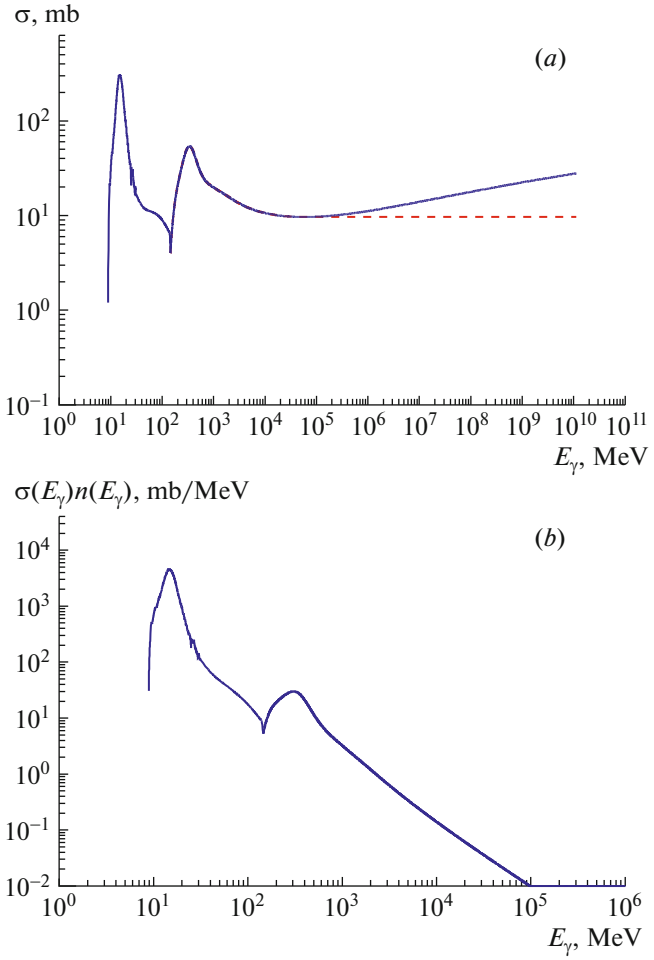

Fig. 3. Total photoabsorption cross section for the ^{129}Xe nucleus and product of it and the spectrum of equivalent photons (both this cross section and this product are used to calculate the total EMD cross section in ^{129}Xe–^{129}Xe collisions at the LHC in the case of the collision energy of $\sqrt{s_{NN}} = 5.44$ TeV): (*a*) photoabsorption cross section for the ^{129}Xe nucleus in the respective E_γ intervals corresponding the data evaluated in the present study ($E_\gamma < 31.2$ MeV), data from the TENDL-2017 library (31.2 MeV $< E_\gamma <$ 140 MeV), and data from the approximations in [16] ($E_\gamma > 145$ MeV) (solid curve) and similar dependences in which the growth of the cross section in the energy region above 60 GeV is disregarded (dashed curve); (*b*) product of the first of the above cross sections and the spectrum of equivalent photons.

gies (versions II and III versus versions IV and V, respectively) turns out to be modest (+1.5%) for the LHC and is more sizable for the FCC-hh (+5%), as might have been expected in view of an increase in the collision energy at the FCC-hh. By and large, agreement between the cross sections obtained by employing data from the TENDL-2017 library and their counterparts evaluated in the present study is found to be fairly good (within 0.5%). At the same time, it should be noted that the RELDIS should be updated by introducing in it newly evaluated total photoabsorption cross sections and by taking into account their growth at photon energies in excess of 60 GeV. On the other hand, the uncertainty in the present calculations with new approximations of photoabsorption cross sections is about 0.6% due to neglecting the two-photon processes. On the whole, the discrepancies between the EMD cross sections for ^{129}Xe that were obtained on the basis of versions I–V of approximations of photoabsorption cross sections do not exceed 8% for the LHC and 13% for the FCC-hh. These results may serve as an estimate of the uncertainty in the calculations of the EMD cross sections for ^{129}Xe nuclei in their collisions at colliders.

5. CONCLUSIONS

On the basis of data available for the ^{127}I nucleus neighboring ^{129}Xe and the combined photonuclear reaction model, we have evaluated the $(\gamma, 1n)$, $(\gamma, 2n)$, $(\gamma, 3n)$, and $(\gamma,$ abs$)$ cross sections for the ^{129}Xe nucleus. We have found that the results of the calculations performed for ^{129}Xe on the basis of this model and with the aid of the TALYS code in the energy region extending up to 40 MeV are close to each other and agree fairly well with Saclay data for ^{127}I. By employing the evaluated data that we obtained, data from the TENDL-2017 library, and the approximations of the total photoabsorption cross sections above the pion production threshold, we have calculated the cross sections for the EMD process in the collisions of ^{129}Xe at the LHC energies and at the energies of the FCC-hh collider being designed. The use of various approximations of total photoabsorption cross sections for the ^{129}Xe nucleus has permitted estimating the uncertainties in the resulting EMD cross sections: 54.6 ± 4 b for the LHC and 76.9 ± 9 b for the FCC-hh. In addition, we have concluded that it is highly desirable to update the RELDIS model by introducing in it the evaluated total photoabsorption cross sections and by taking into account their growth at high energies.

In order to test the EMD cross sections calculated in the present study for ^{129}Xe nuclei, it is advisable to measure the absolute value of this cross section at the LHC. Direct measurements of photoneutron cross sections in a photon beam by employing, for example, a target from liquified ^{129}Xe are very expensive, and—as far as we know—there are no plans at the present time to perform such measurements.

FUNDING

This work was supported under the IAEA (International Atomic Energy Agency) research contract

no. 20501 (Coordination research project no. F41032) and by the BASIS Foundation for the Development of Theoretical Physics and Mathematics (grant no. 18-2-6-93-1).

REFERENCES

1. T. A. Trainor, Int. J. Mod. Phys. E **23**, 1430011 (2014).
2. H. Bello, A. Fernandez, and A. Ortiz, J. Phys.: Conf. Ser. **761**, 012033 (2016).
3. G. E. Bruno, EPJ Web Conf. **95**, 06001 (2015).
4. M. Mackowiak-Pawlowska, Nucl. Phys. A **956**, 344 (2016).
5. J. M. Jowett, J. Phys. G **35**, 104028 (2008).
6. Z. Citron, A. Dainese, J. F. Grosse-Oetringhaus, J. M. Jowett, Y.-J. Lee, U. A. Wiedemann, M. Winn, A. Andronic, F. Bellini, E. Bruna, E. Chapon, H. Dembinski, D. d'Enterria, I. Grabowska-Bold, G. M. Innocenti, C. Loizides, et al., arXiv: 1812.06772.
7. V. Toivanen, G. Bellodi, C. Fichera, D. Küchler, A. M. Lombardi, M. Maintrot, A. Michet, M. O'Neil, S. Sadovich, F. Wenander, and O. Tarvainen, in *Proceedings of the ECRIS2016, Busan, Korea, 28 Aug.–1 Sep. 2016, 2017,* WEAO01.
8. R. Bruce, D. Bocian, S. Gilardoni, and J. M. Jowett, Phys. Rev. ST Accel. Beams **12**, 071002 (2009).
9. I. A. Pshenichnov, Phys. Part. Nucl. **42**, 215 (2011).
10. ALICE Collab. (B. Abelev et al.), Phys. Rev. Lett. **109**, 252302 (2012).
11. C. Bertulani and G. Baur, Phys. Rep. **163**, 299 (1988).
12. V. Guzey, E. Kryshen, and M. Zhalov, Phys. Lett. B **782**, 251 (2018).
13. B. S. Ishkhanov and V. N. Orlin, Phys. Part. Nucl. **38**, 232 (2007).
14. B. S. Ishkhanov and V. N. Orlin, Phys. At. Nucl. **71**, 493 (2008).
15. A. Koning and D. Rochman, Nucl. Data Sheets **113**, 2841 (2012).
16. M. Kossov, Eur. Phys. J. A **14**, 377 (2002).
17. M. Schaumann, Phys. Rev. ST Accel. Beams **18**, 091002 (2015).
18. R. L. Bramblett, J. T. Caldwell, B. L. Berman, R. R. Harvey, and S. C. Fultz, Phys. Rev. **148**, 1198 (1966).
19. R. Bergère, H. Beil, P. Carlos, and A. Veyssière, Nucl. Phys. A **133**, 417 (1969).
20. A. Lepretre, H. Beil, R. Bergère, P. Carlos, J. Fagot, A. De Miniac, A. Veyssière, and H. Miyase, Nucl. Phys. A **258**, 350 (1976).
21. B. L. Berman, R. L. Bramblett, J. T. Caldwell, H. S. Davis, M. A. Kelly, and S. C. Fultz, Phys. Rev. **177**, 1745(1969).
22. A. Lepretre, H. Beil, R. Bergère, P. Carlos, A. de Miniac, A. Veyssière, and K. Kernbach, Nucl. Phys. A **219**, 39 (1974).
23. B. L. Berman, S. C. Fultz, J. T. Caldwell, M. A. Kelly, and S. S. Dietrich, Phys. Rev. C **2**, 2318 (1970).
24. V. V. Varlamov, B. S. Ishkhanov, V. N. Orlin, and S. Yu. Troshchiev, Bull. Russ. Acad. Sci.: Phys. **74**, 842 (2010).
25. V. V. Varlamov, B. S. Ishkhanov, and V. N. Orlin, Phys. At. Nucl. **75**, 1339 (2012).
26. V. V. Varlamov, B. S. Ishkhanov, V. N. Orlin, and K. A. Stopani, Eur. Phys. J. A **50**, 114 (2014).
27. B. S. Ishkhanov, V. N. Orlin, and V. V. Varlamov, EPJ Web Conf. **38**, 1203 (2012).
28. V. V. Varlamov, B. S. Ishkhanov, V. N. Orlin, N. N. Peskov, and M. E. Stepanov, Phys. At. Nucl. **76**, 1403 (2013).
29. V. V. Varlamov, M. A. Makarov, N. N. Peskov, and M. E. Stepanov, Phys. At. Nucl. **78**, 634 (2015).
30. V. V. Varlamov, M. A. Makarov, N. N. Peskov, and M. E. Stepanov, Phys. At. Nucl. **78**, 746 (2015).
31. V. V. Varlamov, A. I. Davydov, M. A. Makarov, V. N. Orlin, and N. N. Peskov, Bull. Russ. Acad. Sci.: Phys. **80**, 317 (2016).
32. V. V. Varlamov, B. S. Ishkhanov, V. N. Orlin, N. N. Peskov, and M. E. Stepanov, Phys. At. Nucl. **79**, 501 (2016).
33. V. V. Varlamov, B. S. Ishkhanov, and V. N. Orlin, Phys. At. Nucl. **80**, 1106 (2017).
34. V. V. Varlamov, V. N. Orlin, and N. N. Peskov, Bull. Russ. Acad. Sci.: Phys. **81**, 670 (2017).
35. Moscow State University Skobeltsyn Institute of Nuclear Physics Centre for Photonuclear Experiments Data, Nuclear Reaction Database (EXFOR). http://cdfe.sinp.msu.ru/exfor/index.php; International Atomic Energy Agency Nuclear Data Section, Database Experimental Nuclear Reaction Data (EXFOR). http://www-nds.iaea.org/exfor; USA National Nuclear Data Center, Database CSISRS and EXFOR Nuclear Reaction Experimental Data. http://www.nndc.bnl.gov/exfor/exfor00.htm.
36. S. S. Dietrich and B. L. Berman, At. Data Nucl. Data Tables **38**, 199 (1988).